ADVANCED FUNCTIONAL MATERIALS
www.afm-journal.de

Real-Time Probing Nanopore-in-Nanogap Plasmonic Coupling Effect on Silver Supercrystals with Surface-Enhanced Raman Spectroscopy

Cong Ma, Qiangqiang Gao, Wei Hong, Jie Fan, and Jixiang Fang**

Nanopore structures have displayed attractive prospects in diverse important applications such as nanopore-based biosensors and enhanced spectroscopy. However, on the one hand, the fabrication techniques to obtain sub-10 nm sized nanopores so far is very limited. On the other hand, the electromagnetic enhancement of nanopores is still relatively low. In this work, using a facile chemical etching strategy on 2D plasmonic Ag nanoparticle supercrystals, fine nanopore arrays with sub-10 nm pore size have been successfully fabricated and a "nanopore-in-nanogap" hybrid plasmon mode has been investigated. An in situ etching and surface-enhanced Raman spectroscopy (SERS) detection indicate that novel hybrid plasmon structure may create an enhanced electromagnetic coupling and increase SERS signal at ≈10× magnification. The breaking of plasmon bonding dipolar mode and generation of antibonding-like plasmon mode contribute to this enhanced electromagnetic coupling. The facile etching strategy, as a common approach, may open the doors for the fabrication of nanopores in various compositions for numerous applications.

1. Introduction

Plasmonics is a flourishing new field of light–matter interactions that exploits the unique optical properties of metallic nanostructures to trap, confine, localize, concentrate, and enhance light at nanometer length scales.[1] In past decades, there are many applications of plasmonics that have emerged like near-field optical microscopy, surface-enhanced Raman spectroscopy (SERS), localized surface plasmon resonance sensing, plasmonic circuitry, active plasmonics, superlenses, surface plasmon lasers, and spacers.[2] Surface plasmons may concentrate light to produce additional high local-field intensities. These locally enhanced fields are often called plasmonic "hot spots".[3] Up to now, different kinds of hot spot sites including nanoparticle (NP) gaps,[4] nanotips,[5] and nanopores[6] have been fabricated. Among them, diverse nanogaps[7–10] such as NP dimmers, trimers, superlattices, planet–satellite structures, NP-on-film, graphene insulated gaps, SHINERS, and various nanotipped structures[11–15] like nanodendrites, nanocorals, nanopolypods, nanostars, nanomeatballs, nanoflowers, and nanourchins have been prepared to create enormous field enhancement.

In comparison with nanogaps and nanotips, nanopores have also attracted a great deal of attention owing to their fascinating potential. For example, nanopore arrays show unexpectedly large transmission at particular wavelengths, a phenomenon known as the extraordinary optical transmission.[16,17] Nanopore sensors have been gaining significant interest due to their single molecule sensitivity and compatibility of detecting a large range of analytes, from DNA and proteins, to small molecules and particles.[18–20] Nanopore arrays have also demonstrated significant high field enhancement due to the combined effects of an intense electromagnetic field generated by the surface plasmons and enhanced light transmission.[21,22] However, currently, some contradictive results upon the influence of pore geometry and dimension on the field enhancement still exist.[23,24] Furthermore, nanopore structures still provide limited enhancement, i.e., typically below 10^5, which are weaker than other reliable SERS substrates.[25] In addition, the fabrication protocols of nanopore arrays have still been exploited to very limited routes such as photolithography, electron beam lithography, and focused ion beam milling.[26,27] In particular, only a few techniques can produce small nanopores down to sub-10 or sub-5 nm scale, which are highly important for the application as nanopore biosensors,[28] e.g., a scanning electron beam nanosculpting is capable of writing nanopores with ≈5 nm features, but not in a massively parallel manner.[29]

C. Ma, Q. Q. Gao, Prof. J. X. Fang
The School of Electronic and Information Engineering
Xi'an Jiaotong University
Shann Xi 710049, P. R. China
E-mail: jxfang@mail.xjtu.edu.cn
C. Ma, Q. Q. Gao
School of Science
Xi'an Jiaotong University
Shann Xi 710049, P. R. China
W. Hong, Prof. J. Fan
Key Lab of Applied Chemistry of Zhejiang Province
Center for Chemistry of High-Performance and Novel Materials
Department of Chemistry
Zhejiang University
Hangzhou 310007, P. R. China
E-mail: jfan@zju.edu.cn

DOI: 10.1002/adfm.201603233

Recently, we have been developing a strategy to prepare highly ordered 2D Ag plasmonic supercrystals and 3D mesoporous Ag superstructures using ordered mesoporous silica as a template through a chemical reduction approach.[30,31] However, it is still challenging for controlled growth of Au or Ag superstructures via nanocasting route because obtained structures may collapse during the removal of templates if no abundant interconnections are formed during reduction stage, thus only nanoparticles, nanowires, or small-sized superstructures are obtained.[32–34] In this work, we modified the nanocasting process reported as our previous approach,[30] utilized 3D ordered mesoporous silica, EP-FDU-12, as hard template, and successfully synthesized large-sized 2D Ag NP supercrystals with nanogap plasmonic mode. Importantly, using an etching process, we purposefully create ultrasmall nanopore microstructure on 2D Ag NP supercrystals by using their periodically nonuniform structure consisting of NPs and particle–particle interfaces. This process has been directly examined by in situ SERS detection due to the four orders of magnitude between SERS signal intensity and electric field strength (SERS~$|E|^{[4]}$). It was found that, as the etching process proceeds, a plasmonic Ag "nanopore-in-nanogap" hybrid structure can be formed and an additional field enhancement can be observed owing to the formation and evolution of nanopores. Electromagnetic field calculation reveals that the formation of nanopores within nanogap region contributes to an enhanced field coupling effect between nanopores and NPs owing to the formation of hybrid plasmon mode.

2. Results and Discussion

In this work, we intend to synthesize large-area 2D Ag supercrystals by means of the nanocasting strategy using ordered mesoporous silica as template (**Figure 1**a) according to below motivations. First, 2D layered structure is preferable since the dispersed supercrystals can easily land on a substrate for further applications. Second, a large area, e.g., larger than 1–2 μm, is necessary for a variety of applications, such as SERS and refractive index sensors. Third, an organic free process via nanocasting process can contribute to a clean metal surface, which is also a critical factor for the sensing applications.

In order to obtain 2D Ag plasmonic supercrystals with larger area, e.g. >1–2 μm, we selected a 3D ordered mesoporous silica, EP-FDU-12, as hard template, which initially was reported by Zhao and co-workers.[35] The scanning electron microscopy (SEM) and the transmission electron microscopy (TEM) images of EP-FDU-12 were shown in Figure S1 (Supporting Information). In particular, compared with commonly used silica template, i.e., KIT-6 or SBA-15, EP-FDU-12 demonstrates a thin wall thickness down to less than 5 nm and a large pore size up to 27 nm. These structural features of EP-FDU-12 display several significant advantages for either nanocasting process or their applications in plasmonic nanooptics. A large pore size may be preferable for nanocasting process since a surface functionalization doesn't need to be requested.[36,37] Furthermore, small nanogaps and large nanoparticle sizes of plasmonic supercrystals can be obtained, which are beneficial to increase the electromagnetic field enhancement.

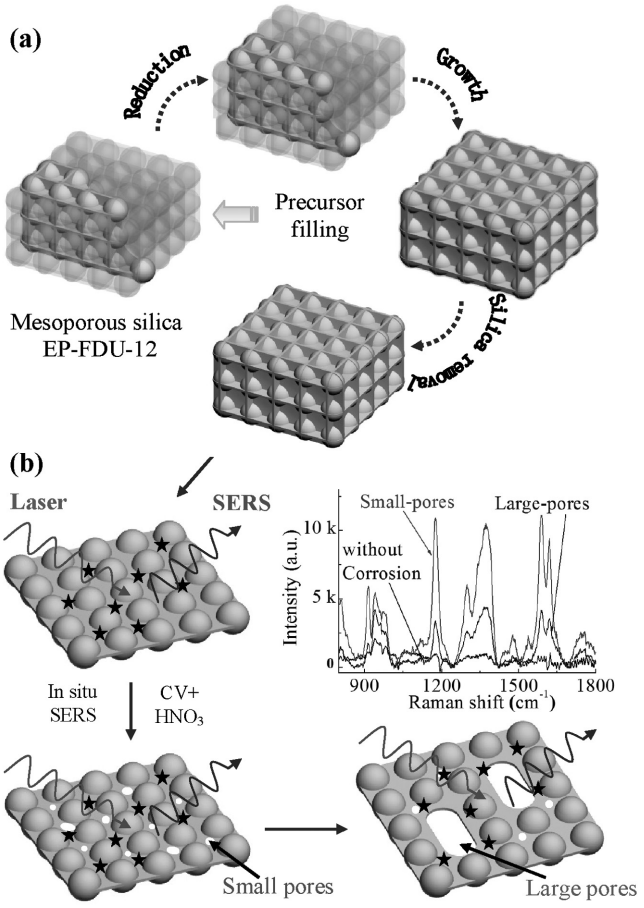

Figure 1. a) A schematic fabrication process of 2D plasmonic Ag NP supercrystals via a nanocasting using mesoporous silica, EP-FDU-12, as template. b) The chemical etching process using HNO_3 aqueous solution and in situ SERS detection.

During the nanocasting processes, SiO_2 template of EP-FDU-12 without surface functionalization was impregnated with $AgNO_3$ precursors. Then compounds of the $AgNO_3$ and SiO_2 template were dried under vacuum condition at 323 K for 12 h. A vacuum reduction is applied to prepare 2D Ag supercrystals using ethylene glycol as the reducing agent. The reduction was carried out at 433 K for 1 h. The increased reduction temperature seems useful to obtain a large area of 2D Ag plasmonic supercrystals. In the following experiments, an etching process was used onto the 2D Ag NP supercrystals to purposefully create multiple plasmon modes. Unexpectedly, it is found that fine nanopores down to sub-10 or sub-5 nm scale have been formed at the early stage of the etching process within nanogap regions as shown in Figure 1b. Thus, we design an in situ SERS detection during the etching process to reveal the influence of formation and evolution of nanopores on the electromagnetic field enhancement (the details can be found in the Experimental Section).

Figure 2 displays the SEM and TEM images of 2D Ag plasmonic supercrystals obtained after the complete removal of mesoporous silica template, EP-FDU-12. Figure 2a is the SEM image of plate-like Ag nanostructures, indicating that the Ag nanostructures are isolated from each other and have an

Adv. Funct. Mater. 2016,
DOI: 10.1002/adfm.201603233

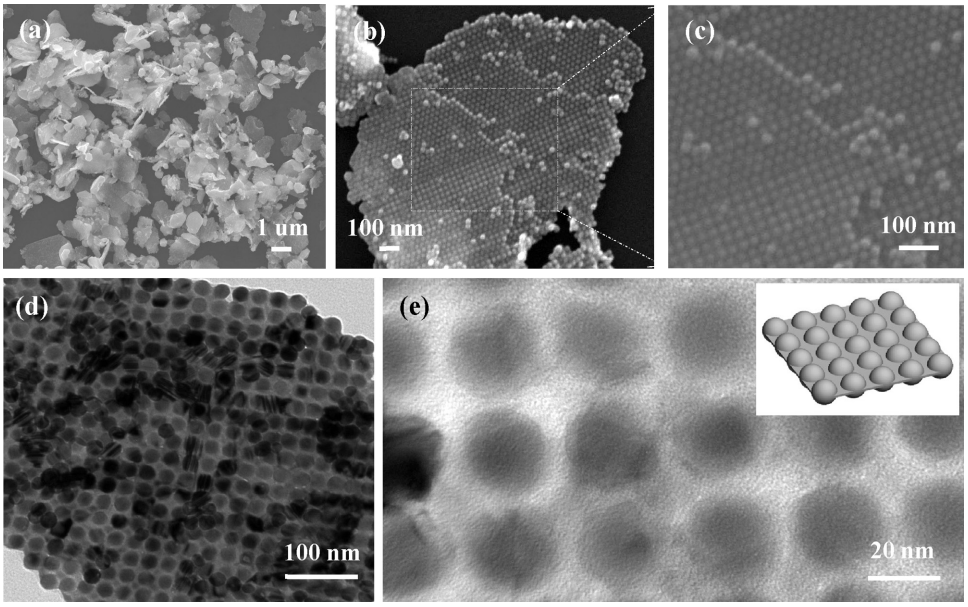

Figure 2. a) Low-magnified, b) high-magnified, and c) enlarged SEM images of 2D Ag NP supercrystals obtained via a nanocasting process using mesoporous silica, EP-FDU-12, as template, d,e) TEM images of 2D Ag NP supercrystals.

average size around 1–2 μm. The individual nanoplate of Ag supercrystals and the enlarged image are shown in Figure 2b,c, which shows a well-organized close-packed NP array consisting of tetragonal and hexagonal arrangement. From Figure 2b, it seems that the individual 2D Ag supercrystals were composed of two or three layers with around 40–60 nm in thickness. The SEM (Figure 2b,c) and TEM (Figure 2d,e) images demonstrate typical structural features, i.e., the uniform NP size distribution of ≈22 nm and the uniformly distributed nanogaps around ≈3 nm between the NPs (Figure 2e). These structural parameters are consistent with the wall thickness and cell size of the parent template. It is noted that no obvious nanopores can be observed within the nanogap region of the 2D Ag supercrystals. A schematic model of 2D Ag supercrystals is shown in the inset of Figure 2e.

In order to evaluate the SERS sensitivity of the 2D Ag plasmonic supercrystals, two kinds of widely used probe molecules, i.e., crystal violet (CV) and 4-aminothiophenol (4-ATP), were detected at ultralow concentrations. To precisely determine the structure of 2D Ag supercrystals and their SERS performance, the same particle was characterized by means of SEM and optical microscopic observations as our previous methods.[30,31] **Figure 3**a is the SERS spectra of CV molecule recorded at 785 nm excitation under various CV concentrations, e.g., from 10^{-7} to 10^{-14} M. The SERS spectra reveal the characteristic peaks of CV molecule, for instance at 1175 and 1588 cm^{-1}, corresponding to the stretching vibrations of ring C—H bend and ring C—C stretching.[38] The limit of detection (LOD) for CV molecule seems down to 10^{-14} M even less (Figure S2, Supporting Information). Figure 3b displays the SERS spectra of 4-ATP adsorbed on 2D Ag supercrystals with the concentrations ranging from 10^{-7} to 10^{-16} M. The SERS spectra of 4-ATP show the characteristic peaks at 1078, 1393, and 1575 cm^{-1}, corresponding to ν(C-S), ν(C-C)+δ(C-H), and δ(C-H), respectively.[39] The Raman signals of CV molecules deviated by less than 12% as shown in Figure S3 (Supporting Information). The CV molecules may uniformly distribute over the entire surface of 2D superstructure proofed by a similar structure (Figure S4, Supporting Information). Again, the LOD of SERS detection for 4-ATP molecule may also reach an ultralow scale, e.g., 10^{-16} M. These results reveal that the obtained 2D Ag plasmonic supercrystals, as SERS active substrate, provide an ultrahigh sensitivity, approaching the capability to detect a single molecule.

As described above, so far, it is still a challenge to fabricate fine nanopores at the sub-10 or sub-5 nm scale, particularly for nanopore arrays, which show great potential for a variety of applications.[16–22] Thus, in order to purposefully create multiple plasmon modes and investigate the influence of nanopores on field coupling modes, an etching process was used onto the 2D Ag NP supercrystals, and this process was monitored by an in situ SERS detection. Before the etching process, the 2D Ag NP supercrystals were immersed into a 10^{-4} M CV aqueous for more than 10 h, so as to absorb CV molecules onto Ag surface. Then the samples were rinsed by dipping in and out pure DI water to remove excess probe molecules and then dropped onto a silicon substrate for etching and in situ SERS measurements, which was conducted within a 10^{-4} M CV and 1×10^{-3} M HNO_3 mixing aqueous solution. **Figure 4** demonstrates the SERS spectra of crystal violet molecule and their evolution during the etching process. Before etching, the SERS peaks of CV molecules show a relatively low intensity owing to the large laser spot size and laser energy loss through aqueous solution. As the etching proceeds, e.g., from 0 to 25 min, the characteristic peaks of CV molecule, i.e., at 1175, 1586, and 1621 cm^{-1}, remarkably increase and reach a maximum intensity at etching time around 25 min as shown in Figure 4a. This SERS intensity is five to ten times higher than the original intensity before the etching treatment. After the etching treatment more than 25 min, the SERS intensity starts to decrease (Figure 4b). When the etching up to 34 min,

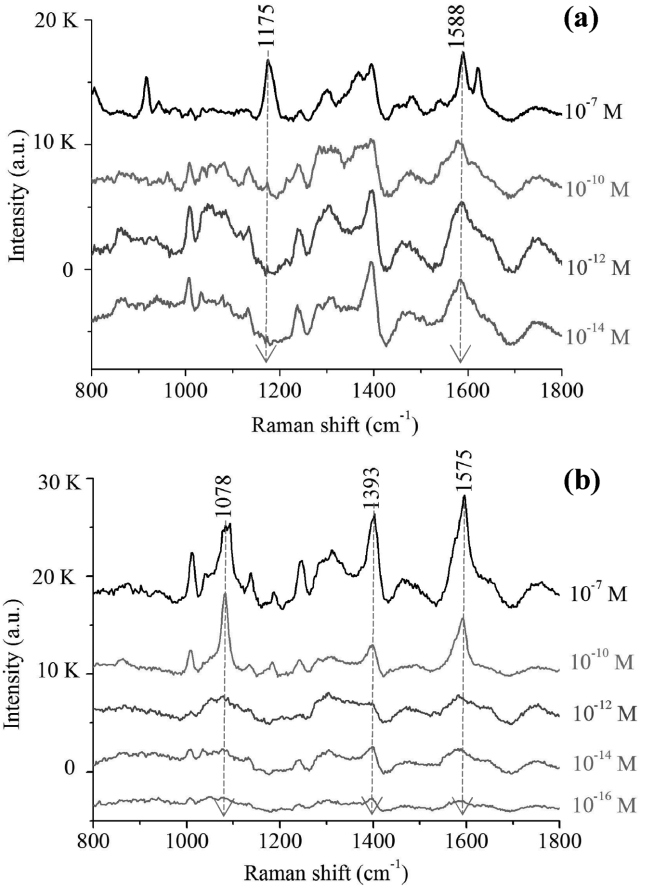

Figure 3. SERS spectra of 2D Ag NP supercrystals with a) crystal violet molecules and b) 4-Aminothiophenol as probes. The SERS spectra are collected at 785 nm excitation 100× objective, 25 mW (5% output) laser power, around 10 µm laser spot size, and 100 s integration time.

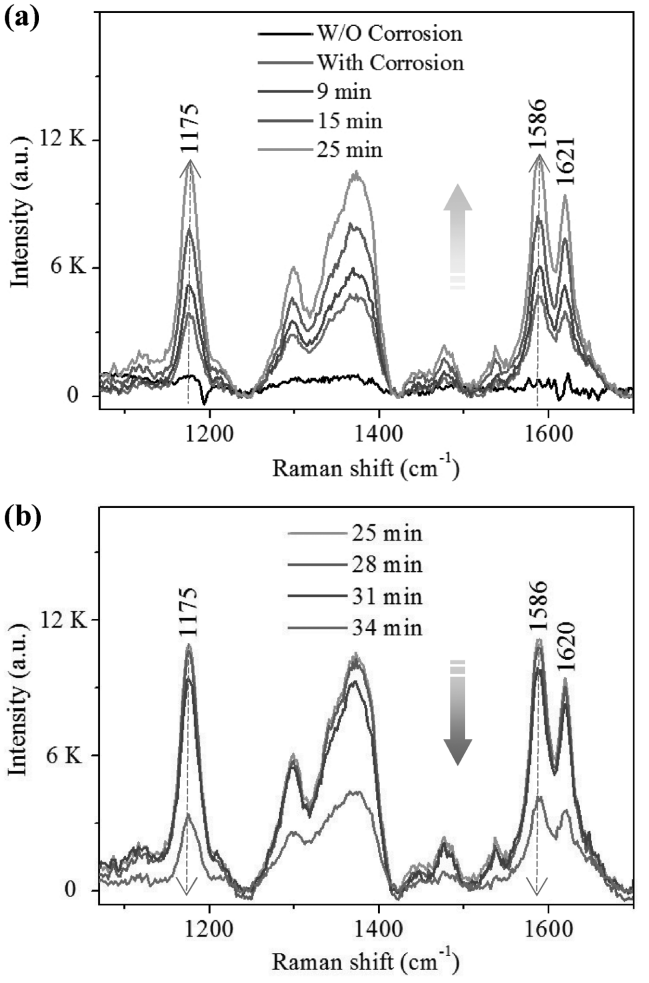

Figure 4. In situ SERS spectra of 2D Ag NP supercrystals with crystal violet molecules as probes during chemical etching process within HNO_3 aqueous solution, a) intensity increasing process, b) intensity decreasing process. The SERS spectra are collected at 785 nm excitation 20× objective, 25 mW (5% output) laser power, 20 µm laser spot size, and 170 s integration time.

the Raman peak intensity has significantly reduced, but still higher than that of original intensity without HNO_3 treatment. The etching-time-dependent SERS enhancement capability can be further proofed by the ex situ SERS measurement as shown in Figure S5 (Supporting Information), in which the 2D Ag NP supercrystals were corroded by different etching time then immersed in CV solution under the same soaking time. One can find that the in situ and ex situ SERS characterizations demonstrate a consistent tendency.

In order to study the origins of the significantly improved SERS performance, the structural change occurring in 2D Ag NP supercrystals during the etching treatment process was studied by analyzing the intermediate specimens taken from the different etching periods using SEM and TEM characterizations. The SEM and TEM images shown in **Figure 5**a,b display a typical structure after etching reaction around 25 min, consisting of many fine nanopores located in the particle–particle interface regions. We called this structure Ag "nanopore-in-nanogap" hybrid arrays. A schematic model of 2D Ag "nanopore-in-nanogap" hybrid arrays is shown in the inset of Figure 5a. In this study, the Ag parts between Ag NPs were gradually etched by HNO_3 solution. However, the Ag NPs were not efficiently etched and their spherical morphologies were maintained through the etching reaction, particularly at the early stage. As the further etching proceeds, some nanopits may be observed as shown in Figure S6 (Supporting Information). When the etching reaction reaches around 28 min (Figure 5c), the Ag hybrid arrays start to collapse, indicating some large pores have been formed. As further increase in the etching time up to 34 min, the large pores can be obviously observed as shown in Figure 5d. This structural evolution processes seem to imply the "nanopore-in-nanogap" hybrid microstructure is favorable to obtain an enhanced electromagnetic field coupling, hence an improved SERS performance.

The underlying physical essence of the influence from "nanopore-in-nanogap" hybrid microstructure on electromagnetic field coupling has been further investigated through finite difference time domain (FDTD) simulations (Figure S7, Supporting Information).[40,41] According to the calculated electromagnetic field (E-fields) intensity and its distribution, when fine nanopores or middle-sized large pores are formed in initial 2D

DOI: 10.1002/adfm.201603233

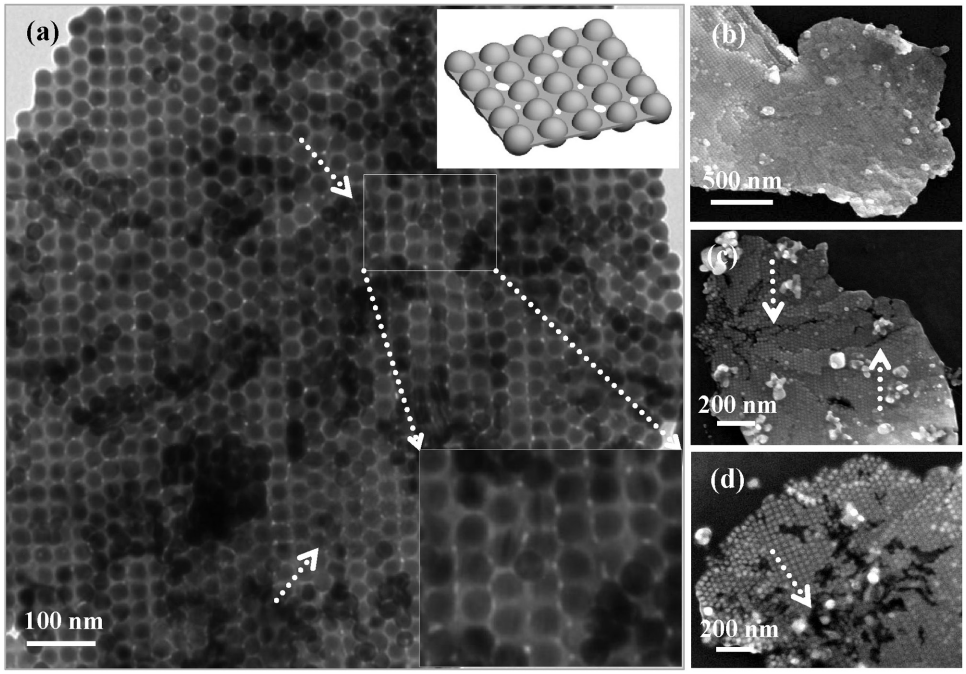

Figure 5. a) TEM images of 2D Ag "nanopore-in-nanogap" hybrid arrays after etching reaction around 25 min using HNO_3 aqueous solution. b–d) SEM images of 2D Ag NP supercrystals after etching reaction of 25, 28, and 34 min, respectively. (White arrows denote nanopores or large pores).

Ag NP supercrystals, the E-fields can be dramatically enhanced, particularly for the case in "nanopore-in-nanogap" hybrid arrays. In comparison to the original intensity value of $|E|^2/|E_0|^2$~45 as shown in **Figure 6**a, the E-fields are enhanced to around 240 and 103 for fine nanopores and middle-sized large pores, respectively. However, when the pores are further etched to more than 40–50 nm, the E-fields intensity in the vicinity of the large nanopores is inversely reduced, e.g., the value of $|E|^2/|E_0|^2$~55.

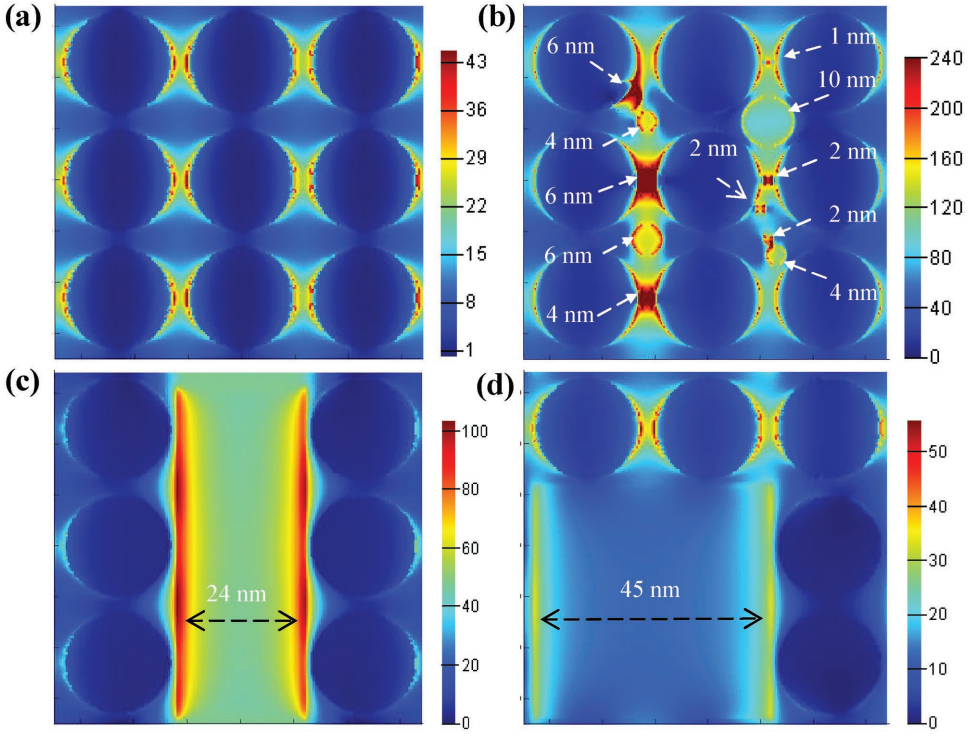

Figure 6. Electric field distribution ($|E|^2/|E_0|^2$) of Ag NP arrays a) without and b) with nanopores at the pore sizes in the range of 1–10 nm, c) with middle large nanopore of 24 nm in size, and d) with large nanopore of 45 nm in size, respectively.

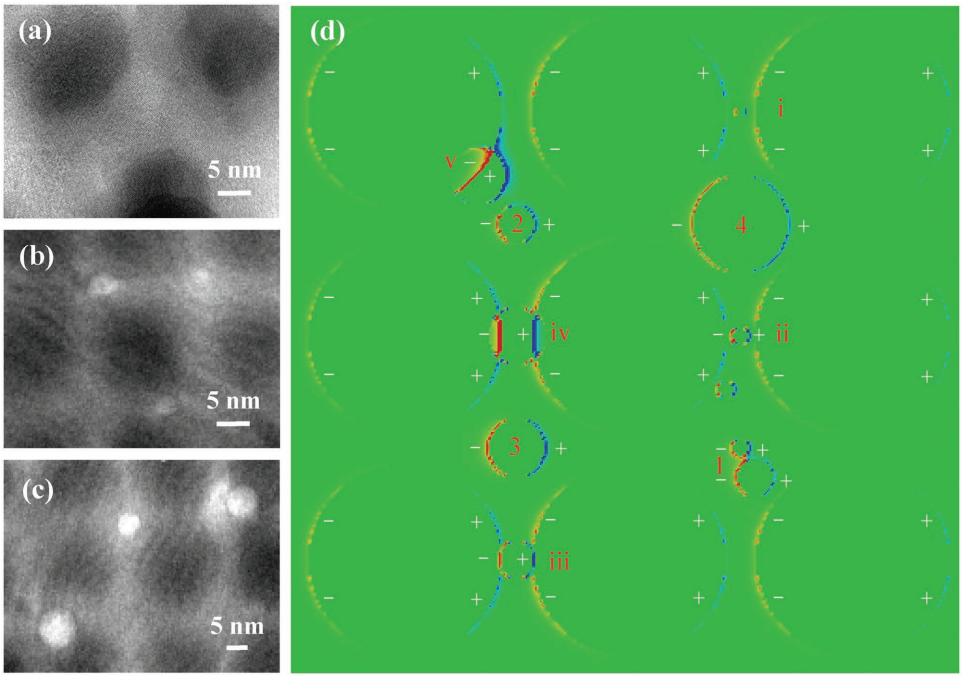

Figure 7. a–c) TEM images of nanopores located at different positions within nanogap regions, and d) the charge distribution of the Ag NP arrays corresponding model as shown in Figure 6b.

If we carefully observed the E-fields of "nanopore-in-nanogap" hybrid arrays (Figure 6b) where the fine nanopores are located at diverse positions, it seems to reveal that the size and position of nanopores may result in quite different influence on E-field enhancement. When nanopores locate at the central region of quadrangle NP arrays, i.e., position '1', '2', '3', and '4' in **Figure 7**d, they contribute to only a relatively weak enhancement. However, when the fine nanopores locate at the neck regions between two NPs, e.g., position 'iii' and 'iv' in Figure 7d, or overlapped regions with NPs, e.g., position 'v' in Figure 7d, the nanopores with larger size (e.g., more than 4 nm) lead to a dramatically enhanced E-fields.

In the actual etching process, the nanopores initially form in the vicinity of particle–particle interfaces, i.e., nanogap regions, but exact position is uncontrollable. The TEM images shown in Figure 7a–c display that the nanopores with sizes of 3–10 nm within "nanopore-in-nanogap" hybrid arrays randomly locate in various positions, such as '1', '2', '3', and '4' or 'ï', 'ii', 'iii' and 'iv', or 'v' in Figure 7d. However, the FDTD results shown in Figure 6b indicate that only some special position and nanopore size, e.g., position 'iii', 'iv', and 'v' can generate largest near-field enhancements. This phenomenon can be further explained via an analysis of surface charge distribution (Figure 7d), corresponding to E-fields distribution shown in Figure 6b. Figure 7d displays that NPs in Ag supercrystals and nanopores located at positions of '1', '2', '3', and '4' present apparent plasmon bonding dipolar mode. Moreover, the surface charge of each unit shows a close loop. While, when nanopores occur at the necks of NPs or at 'v' position (Figure 7d) and pore size is larger (e.g., >4 nm), surface charge loop is broken, thus generating an antibonding-like plasmon mode. The surface charges at the broken segments are opposed, leading to a hybrid plasmon mode, which acts to increase the magnitudes of the E-fields in those areas.[42] Therefore, the nanopore position and size-dependent E-fields enhancement is obtained.

In the actual etching process, some fine roughness features can be created, which may also be severe as localized plasmonic "hot spots" to contribute to additional electromagnetic enhancement. In this study, we cannot exclude the importance of etched rough microstructures, e.g., nanopits, except for nanopores, owing to simultaneously creating the nanopores and nanopits. Therefore, we investigated the influence of nanopits on the electromagnetic enhancement and distribution using the FDTD simulations (Figure S8, Supporting Information). According to the results shown in Figure S6 and Figure S9 (Supporting Information), the model combining nanogaps and nanopits does not increase the field enhancement comparing the model with only nanogaps. It reveals that the maximum field enhancement still occurs at the position of nanogaps. Similarly, the introduction of nanopits into the model of Figure 6b cannot increase the field enhancement, and the maximum field enhancement still localizes at the "nanopore-in-nanogap" position (Figure S10, Supporting Information). These results indicate that the current enhanced response mainly originates from the "nanopore-in-nanogap" plasmon coupling mode. In fact, Chen and co-workers have also found that the strongest SERS enhancement of nanoporous gold takes place from the samples with an ultrafine nanopore size of ≈5–10 nm.[43] It seems to reveal that nanopores, by means of an optimized design, e.g., its size and position, may be exploited to obtain a huge field enhancement.

Up to now, many kinds of electromagnetic enhancement structures have been successfully exploited for various applications, e.g., in SERS. For example, using lithography technique

DOI: 10.1002/adfm.201603233

combining metallic deposition, Fang et al., Wu et al., and Im et al. successfully fabricated different nanogap arrays, respectively.[44–46] These patterning techniques indeed can improve the uniformity and reproducibility of the SERS signal. However, the high cost and low throughput by these lithographic protocols are really disadvantageous for the marketing of the SERS technique. Therefore, in recent decades, exciting successes have been achieved using colloid chemistry strategy to well define nanogaps. For instant, using DNA-directed method, Au-Ag core–shell nanodumbbells and Au nanobridged nanogap particles have been successfully synthesized.[47,48] These structures demonstrated outstanding nanogap control. In addition, 3D plasmonic nanoclusters and $Au/SiO_2/Au$ nanoshells can provide a high degree of plasmonic tenability by means of tuning the particle number and internal geometry.[49,50] Besides, above lithography and colloid chemistry routes, the dealloying process may fabricate porous Au-Ag alloy nanostructures, which showed a remarkable SERS property.[43,51]

In this study, the 2D Ag NP supercrystals can be used as high-quality SERS substrates. Compared with the above reported typical SERS substrates, 2D Ag supercrystals were fabricated via nanocasting process. This process, unlike colloidal nanoparticles aggregate randomly during drying, prevents the nanoparticle from the "coffee-ring" effect. Thus, 2D Ag supercrystals demonstrate an active plasmonic array structure with high density and uniform nanogaps of ≈3 nm between nanoparticles. Furthermore, using the current chemical etching protocol, a "nanopore-in-nanogap" hybrid plasmon mode can be created, which contributes to an additional electromagnetic enhancement. However, some disadvantages and limitations of 2D Ag supercrystals are still opening. For example, the size uniformity of Ag supercrystals is still needed to be improved to meet the signal uniform of SERS detection. In addition, the randomly attached nanoparticles on the surface of 2D Ag supercrystals may also influence the electromagnetic field enhancement. Thus, great efforts would be devoted to solve these issues.

3. Conclusions

In summary, we have successfully fabricated sub-10 nm sized nanopore arrays by means of a facile chemical etching process on 2D plasmonic Ag NP supercrystals. Using in situ SERS detection, the formation and evolution of nanopores have been directly examined and the influence of nanopores on the electromagnetic field coupling effect has been investigated. First, using a nanocasting strategy, utilized 3D ordered mesoporous silica, EP-FDU-12, as hard template, large-sized 2D Ag NP supercrystals have been synthesized. The plasmonic Ag supercrystals are composed of NP building units with around 22 nm in size and uniform nanogaps of ≈3 nm. Second, using a chemical etching process with HNO_3 aqueous solution, a "nanopore-in-nanogap" hybrid plasmon mode has been formed. This novel hybrid plasmon mode generates an additional enhanced electromagnetic coupling effect and results in ≈10× magnification of SERS signal. Third, electromagnetic field calculation using FDTD method reveals that the position and size of nanopores in "nanopore-in-nanogap" structure have an important role in E-fields coupling. When the nanopores locate at the necks between NPs or overlapped regions with NPs, surface charge loop is broken and an antibonding-like plasmon mode is formed, which contributes to an enhanced E-fields. Therefore, the current protocol not only exploits a new approach to fabricate nanopore arrays with sub-10 nm scale, but also opens a route to explore diverse novel applications in plasmon enhanced spectroscopy as well as nanopore-based biosensors in DNA and protein analysis.[18–20]

Supporting Information

Supporting Information is available from the Wiley Online Library or from the author.

Acknowledgements

J. X. Fang was supported by National Natural Science Foundation of China (Grant No. 21675122), Doctoral Fund of Ministry of Education of China (Grant No. 20130201110032), and the Fundamental Research Funds for the Central Universities (Grant No. xkjc2014004).

Received: June 28, 2016
Revised: October 2, 2016
Published online:

[1] J. A. Schuller, E. S. Barnard, W. S. Cai, Y. C. Jun, J. S. While, M. L. Brongersma, *Nat. Mater.* **2010**, *9*, 193.
[2] Z. Y. Fang, X. Zhu, *Adv. Mater.* **2013**, *25*, 3840.
[3] H. X. Xu, J. Aizpurua, M. Kall, P. Apell, *Phys. Rev. E* **2000**, *62*, 4318.
[4] H. X. Xu, E. J. Bjerneld, M. Kall, L. Borjesson, *Phys. Rev. Lett.* **1999**, *83*, 4357.
[5] E. Hao, R. C. Bailey, G. C. Schatz, J. T. Hupp, S. Y. Li, *Nano Lett.* **2004**, *4*, 327.
[6] A. G. Brolo, E. Arctander, R. Gordon, B. Leathem, K. L. Kavanagh, *Nano Lett.* **2004**, *4*, 2015.
[7] H. Wang, L. Y. Chen, X. H. Shen, L. F. Zhu, J. T. He, H. Y. Chen, *Angew. Chem. Int. Ed.* **2012**, *51*, 8021.
[8] A. Q. Fang, S. White, P. K. Jain, F. P. Zamborini, *Nano Lett.* **2015**, *15*, 542.
[9] J. F. Li, Y. F. Huang, Y. Ding, Z. L. Wang, S. B. Li, X. S. Zhou, F. R. Fan, W. Zhang, Z. Y. Zhou, D. Y. Wu, B. Ren, Z. L. Wang, Z. Q. Tian, *Nature* **2010**, *464*, 392.
[10] J. Mertens, A. L. Eiden, D. O. Sigle, F. M. Huang, A. Lombardo, Z. P. Sun, R. S. Sundaram, A. Colli, C. Tserkezis, J. Aizpurua, S. Milana, A. C. Ferrari, J. J. Baumberg, *Nano Lett.* **2013**, *13*, 5033.
[11] Z. Liu, Z. B. Yang, B. Peng, C. Cao, C. Zhang, H. J. You, Q. H. Xiong, Z. Y. Li, J. X. Fang, *Adv. Mater.* **2014**, *26*, 2431.
[12] Z. Liu, L. Cheng, L. Zhang, Z. B. Yang, Z. Liu, J. X. Fang, *Biomaterials* **2014**, *35*, 4099.
[13] Z. Liu, F. L. Zhang, Z. B. Yang, H. J. You, C. F. Tian, Z. Y. Li, J. X. Fang, *J. Mater. Chem. C* **2013**, *1*, 5567.
[14] J. X. Fang, S. Y. Du, Z. Y. Li, S. Lebedkin, R. Kruk, H. Hahn, *Nano Lett.* **2010**, *10*, 5006.
[15] Z. Liu, L. Zhang, C. Jing, X. Shi, Z. B. Yang, Y. T. Long, J. X. Fang, *Nanoscale* **2014**, *6*, 2567.
[16] T. W. Ebbesen, H. J. Lezec, H. F. Ghaemi, T. Thio, P. A. Wolff, *Nature* **1998**, *391*, 667.

[17] C. Genet, T. W. Ebbesen, *Nature* **2007**, *445*, 39.
[18] F. Haque, J. H. Li, H. C. Wu, X. J. Liang, P. X. Guo, *Nano Today* **2013**, *8*, 56.
[19] Q. Zhao, G. Sigalov, V. Dimitrov, B. Dorvel, U. Mirsaldov, S. Sligar, A. Aksimentiev, G. Timp, *Nano Lett.* **2007**, *7*, 1680.
[20] M. Wanunu, J. Sutin, A. Meller, *Nano Lett.* **2009**, *9*, 3498.
[21] H. Rigneault, J. Capoulade, J. Dintinger, J. Wenger, N. Bonod, E. Popov, T. W. Ebbesen, P. F. Lenne, *Phys. Rev. Lett.* **2005**, *95*, 117401.
[22] F. J. Garcia-vidal, L. M.-Moreno, T. W. Ebbesen, *L. Kuipers, Rev. Mod. Phys.* **2010**, *82*, 729.
[23] S. O. Kucheyev, J. R. Hayes, J. Biener, T. Huser, C. E. Talley, A. V. Hamza, *Appl. Phys. Lett.* **2006**, *89*, 053102.
[24] L. H. Qian, X. Q. Yan, T. Fujita, A. Inoue, M. W. Chen, *Appl. Phys. Lett.* **2007**, *90*, 153120.
[25] Q. M. Yu, P. Guan, Q. Dong, G. Golden, P. M. Wallace, *Nano Lett.* **2008**, *8*, 1923.
[26] Y. Li, F. Nicoli, C. Chen, L. Iagae, G. Groeseneken, T. Stakenborg, H. W. Zandbergen, C. Dekker, P. V. Dorpe, M. P. Jonsson, *Nano Lett.* **2015**, *15*, 776.
[27] G. Ando, C. Hyun, J. L. Li, T. Mitsui, *ACS Nano* **2012**, *6*, 10090.
[28] B. M. Venkatesan, R. Bashir, *Nat. Nanotechnol.* **2011**, *6*, 615.
[29] M. D. Fishbein, *M. Drndic. Appl. Phys. Lett.* **2008**, *93*, 113107.
[30] C. F. Tian, Y. H. Deng, D. Y. Zhao, J. X. Fang, *Adv. Opt. Mater.* **2015**, *3*, 404.
[31] C. F. Tian, J. Li, C. S. Ma, P. Wang, X. H. Sun, J. X. Fang, *Nanoscale* **2015**, *7*, 12318.
[32] A. Takai, Y. Doi, Y. Yamauchi, K. Kuroda, *J. Phys. Chem. C.* **2010**, *114*, 7586.
[33] Z. Li, C. Kubel, V. I. Parvulescu, R. Richards, *ACS Nano* **2008**, *2*, 1205.
[34] Z. W. Liu, R. C. Che, A. A. Elzatahry, D. Y. Zhao, *ACS Nano* **2014**, *8*, 10455.
[35] J. Fan, C. Z. Yu, J. Lei, Q. Zhang, T. C. Li, B. Tu, W. Z. Zhou, D. Y. Zhao, *J. Am. Chem. Soc.* **2007**, *127*, 10794.
[36] J. K. Shon, S. S. Kong, J. M. Kim, C. H. Ko, M. S. Jin, Y. Y. Lee, S. H. Hwang, J. A. Yoon, J. N. Kim, *Chem. Comm.* **2009**, *6*, 650.
[37] M. Kitahara, K. Kuroda, *RSC Adv.* **2014**, *4*, 27201.
[38] J. X. Fang, S. Y. Liu, Z. Y. Li, *Biomaterials* **2011**, *32*, 4877.
[39] A. Gopinath, S. V. Boriskina, W. R. Premasiri, L. Ziegler, B. M. Reinhard, L. D. Negro, *Nano Lett.* **2009**, *9*, 3922.
[40] C. F. Tian, C. H. Ding, S. Y. Liu, S. C. Yang, X. P. Song, B. J. Ding, Z. Y. Li, J. X. Fang, *ACS Nano* **2011**, *5*, 9442.
[41] L. Cheng, C. S. Ma, G. Yang, H. J. You, J. X. Fang, *J. Mater. Chem. A* **2014**, *2*, 4534.
[42] A. W. Clark, J. M. Cooper, *Adv. Mater.* **2010**, *22*, 4025.
[43] L. H. Qian, X. Q. Yan, T. Fujita, A. Inoue, *M. W. Chen. Appl. Phys. Lett.* **2007**, *90*, 153120.
[44] Y. Fang, N. Seong, D. D. Dlott, *Science* **2008**, *321*, 388.
[45] H. Y. Wu, C. J. Choi, B. T. Cunningham, *Small* **2012**, *8*, 2878.
[46] H. Im, K. C. Bantz, N. C. Lindquist, C. L. Haynes, S. H. Oh, *Nano Lett.* **2010**, *10*, 2231.
[47] D. K. Lim, K. S. Jeon, H. M. Kim, J. M. Nam, Y. D. Suh, *Nat. Mater.* **2010**, *9*, 60.
[48] D. K. Lim, K. S. Jeon, J. Hwang, H. Kim, S. Kwon, Y. D. Suh, J. Nam, *Nat. Nanotechnol.* **2011**, *6*, 452.
[49] A. S. Urban, X. S. Shen, Y. M. Wang, N. Large, H. Wang, M. W. Knight, P. Nordlander, H. Y. Chen, N. J. Halas, *Nano Lett.* **2013**, *13*, 4399.
[50] R. Bardhan, S. Mukherjee, N. A. Mirin, S. D. Levit, P. Nordlander, N. J. Halas, *J. Phys. Chem. C.* **2010**, *114*, 7378.
[51] K. Liu, Y. C. Bai, L. Zhang, Z. B. Yang, Q. K. Fan, H. Q. Zheng, Y. D. Yin, C. B. Gao, *Nano Lett.* **2016**, *16*, 3675.

Adv. Funct. Mater. **2016**,
DOI: 10.1002/adfm.201603233